This is the Pre-Published Version.

This is the peer reviewed version of the following article: Zheng, Y., Wei, H., Liang, P., Xu, X., Zhang, X., Li, H., ... & Zhuang, J. (2021). Near-infrared-excited multicolor afterglow in carbon dots-based room-temperature afterglow materials. Angewandte Chemie, 133(41), 22427-22433, which has been published in final form at https://doi.org/10.1002/anie.202108696. This article may be used for non-commercial purposes in accordance with Wiley Terms and Conditions for Use of Self-Archived Versions. This article may not be enhanced, enriched or otherwise transformed into a derivative work, without express permission from Wiley or by statutory rights under applicable legislation. Copyright notices must not be removed, obscured or modified. The article must be linked to Wiley's version of record on Wiley Online Library and any embedding, framing or otherwise making available the article or pages thereof by third parties from platforms, services and websites other than Wiley Online Library must be prohibited.

Near-Infrared-Excited Multicolor Afterglow in Carbon Dots-Based Room-Temperature Afterglow Materials

Yihao Zheng[+a,b], Haopeng Wei[+a,b], Ping Liang[a,b], Xiaokai Xu[a,b], Xingcai Zhang[c,d], Huihong Li[a], Chenlu Zhang[a], Chaofan Hu[a,b], Xuejie Zhang[a,b], Bingfu Lei[a,b], Wai-Yeung Wong[e], Yingliang Liu*[a,b], and Jianle Zhuang*[a,b]*

[a] Key Laboratory for Biobased Materials and Energy of Ministry of Education/Guangdong Provincial Engineering Technology Research Center for Optical Agriculture, College of Materials and Energy, South China Agricultural University, Guangzhou 510642, China. Email: tliuyl@scau.edu.cn, zhuangjl@scau.edu.cn

[b] Guangdong Laboratory for Lingnan Modern Agriculture, Guangzhou 510642, China

[c] School of Engineering and Applied Sciences, Harvard University, Cambridge, MA, 02138, USA

[d] School of Engineering, Massachusetts Institute of Technology, Cambridge, MA, 02139, USA

[e] Department of Applied Biology and Chemical Technology, The Hong Kong Polytechnic University, Hung Hom, Hong Kong, China and Hong Kong Polytechnic University Shenzhen Research Institute, Shenzhen 518057, China. E-mail: wai-yeung.wong@polyu.edu.hk

[+] These authors contributed equally to this work.

Abstract: *Room-temperature afterglow (RTA) materials with long lifetime have shown tremendous application prospects in many fields. However, there is no general design strategy to construct near-infrared (NIR)-excited multicolor RTA materials. Herein, we report a universal approach based on the efficient radiative energy transfer that supports the reabsorption from upconversion materials (UMs) to carbon dots-based RTA materials (CDAMs). Thus, the afterglow emission (blue, cyan, green, and orange) of various CDAMs can be activated by UMs under the NIR continuous-wave laser excitation. The efficient radiative energy transfer ensured the persistent multicolor afterglow up to 7 s, 6 s, 5 s, and 0.5 s by naked eyes, respectively. Given the unusual afterglow properties, we demonstrated preliminary applications in fingerprint recognition and information security. This work provides a new avenue for the activation of NIR-excited afterglow in CDAMs and will greatly expand the applications of R TA.*

Room-temperature afterglow (RTA) materials refer to a type of long-lived luminescent materials that absorb energy at room temperature and still show afterglow after the radiation is shut off.[1] Long-lived emission can eliminate the interference of background fluorescence and light scattering,[2] which entitles RTA materials with irreplaceable advantages in diverse applications such as anti-counterfeiting, sensing, information encryption, optoelectronic devices, and biological imaging, compared to fluorescent materials.[3] In recent years, the RTA phenomena have been continuously discovered in carbon dots (CDs).[4] As a new kind of RTA materials, CDs-based RTA materials (CDAMs) have advantages of superior afterglow properties, facile preparation, low toxicity, good stability and biocompatibility, and ease of structural regulation.[5] Therefore, CDAMs are becoming more promising in a wide range of practical applications.[4]

With the emergence of various CDAMs, much effort has been devoted to the regulation and optimization of their RTA properties. The afterglow emission color range has been extended from blue to red when CDs are embedded into various matrices, such as polymers,[6] melamine,[7] cyanuric acid,[8] sodium chloride,[9] aluminum sulfate,[10] zeolite,[11] layer double hydroxide,[12] silica,[13] urea,[14] and boric acid.[15] These studies indicate that great progress has been made in tuning the RTA emission wavelength in CDAMs. However, the tuning of the excitation wavelength of CDAMs remains a great challenge. Most of the reported CDAMs can only be excited by ultraviolet (UV) light.[4] Even if some of them can be excited by visible light, it is due to the excitation dependence property of CDs, and their quantum efficiencies are very low.[16] In fact, there are very limited reports about visible-light-excited afterglow in CDAMs.[17] The characteristic of being excited only by UV or visible light severely limits the further applications of CDAMs. As we know, near-infrared (NIR) light has lower energy, less light damage, and deeper penetration, which shows attractive application especially in the field of anti-counterfeiting, information encryption, and biological imaging.[18] However, up to now, there is no report about the NIR-excited afterglow in CDAMs. Therefore, it is of great importance to develop CDAMs which can be excited by the NIR light.

Herein, we propose an innovative and universal design strategy (Scheme 1), ingeniously using upconversion materials (UMs), which can convert NIR light to UV or visible light,[19] to activate the afterglow of CDAMs under the near-infrared continuous-wave (NIR CW) laser excitation at 980 nm. In detail, $NaYF_4$:Yb,Tm UMs were synthesized as the energy donor, which can emit strong UV and blue light under CW laser excitation at 980 nm. Subsequently, four different kinds of CDAMs as the acceptor absorbed the emitted light from UMs to exhibit multicolor (blue, cyan, green, and orange) afterglow.

Furthermore, the energy transfer mechanism of the activation process was proved to be radiative energy transfer through the related steady-state and transient spectra. Finally, the NIR-excited multicolor afterglow of CDAMs was successfully used for fingerprint recognition, 4D code, and optical anti-counterfeiting signatures, which greatly improved information recognition and encryption level. Note that this is the first report of the NIR-excited multicolor afterglow in CDAMs. More importantly, this work provides a universal route to the construction of new RTA materials with tunable excitation wavelengths.

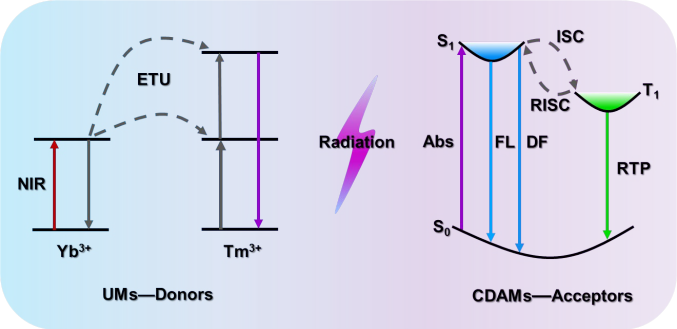

Scheme 1. Simplified schematic illustration of activating the multicolor afterglow of CDAMs under the NIR CW laser excitation.

Multicolor and long-lived CDs-based RTA materials (CDAMs) with excellent performance were synthesized by the facile and fast bottom-up methods using small-molecule chemicals (see the experimental section in the Supporting Information). Their morphologies were firstly characterized by the transmission electron microscope (TEM). As shown in Figure 1a-d, four kinds of CDs contained in the four CDAMs matrices exhibit uniform and well dispersed quasi-spherical morphologies with average sizes of about 2.0 nm, 2.3 nm, 2.0 nm, and 2.1 nm, respectively (Figure S1). The high-resolution (HR) TEM images in the insets of Figure 1a-d show that the lattice spacing of CDs is about 0.21 nm, which corresponds to the (100) plane of graphitized carbon.[20] The X-ray diffraction (XRD) patterns display same diffraction peaks for B-CDAMs, C-CDAMs, and G-CDAMs, which can be attributed to the formation of boron oxide during the boric acid coating process (Figure S2a).[15] The Fourier transform infrared (FT-IR) spectra demonstrate characteristic absorption bands for B-CDAMs, C-CDAMs, and G-CDAMs, which were assigned to -OH (3225 cm^{-1}), B-O (1475 cm^{-1}), B-O-H (1205 cm^{-1}), B-O-C (1060 cm^{-1}), and B-C (950 cm^{-1}) stretching vibrations, respectively (Figure S2b).[15] Since urea is used as the matrix, different characteristics are presented in the XRD pattern for O-CDAMs (Figure S2a). The FT-IR spectrum of O-CDAMs exhibits characteristic absorption bands for N-H (3465 cm^{-1}), C=O (1740 cm^{-}

^{1}), C=C (1637 cm^{-1}), and C-N (1469 cm^{-1}) stretching vibrations, respectively (Figure S2b).[14a] The characteristic of CDs can be further proved by the X-ray photoelectron spectroscopy (XPS) results (Figure S3).[21] Optical properties of CDAMs were characterized by afterglow emission spectra and UV-vis absorption spectra. The normalized afterglow emission spectra in Figure 1e exhibited the highest emissive peaks of the four kinds of CDAMs at 425 nm, 477 nm, 506 nm, and 598 nm, respectively. As seen from Figure 1f, these CDAMs show bright afterglow from blue to orange after turning off the 365 nm UV lamp. The absorption spectra in Figure 1g demonstrate that these four kinds of CDAMs have intense absorption in the UV and blue regions. Their RTA lifetimes from B-CDAMs to O-CDAMs were determined to be 1.82 s, 0.80 s, 1.85 s, and 0.12 s, respectively (Figure 1h). In addition, more detailed fluorescence spectra, afterglow emission spectra, and afterglow emission spectra at different temperatures can be found in Figure S4-6. It is worth mentioning that all four CDAMs show no upconversion luminescence (UCL) under the NIR CW laser excitation at 980 nm (Figure S7), which was the original intention and significance of activating afterglow of CDAMs in this work.

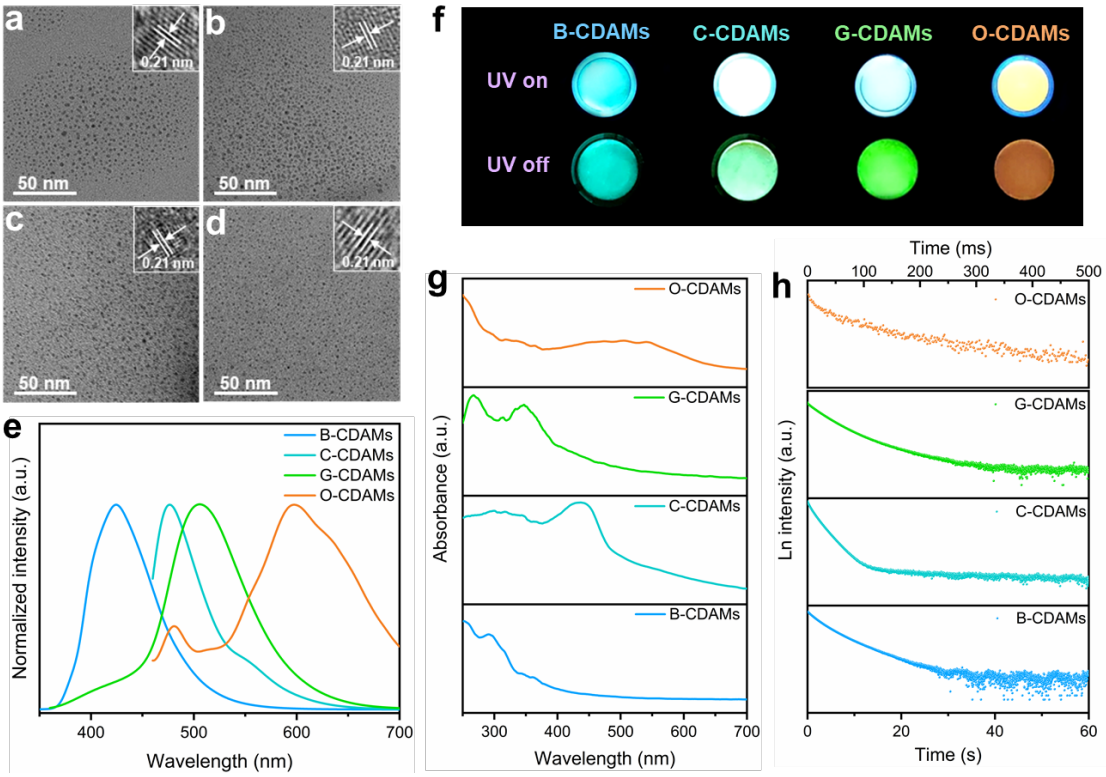

Figure 1. TEM images of the as-synthesized a) B-CDAMs, b) C-CDAMs, c) G-CDAMs, and d) O-CDAMs; the insets are the HRTEM images corresponding to CDs. e) Normalized afterglow emission spectra of B-CDAMs, C-CDAMs, G-CDAMs, and O-CDAMs under the optimal excitation at 260 nm, 440 nm, 340 nm, 440 nm, respectively. f) Photographs of B-CDAMs, C-CDAMs, G-CDAMs, and O-

CDAMs with the UV lamp on and off at 365 nm. g) UV-vis absorption spectra of B-CDAMs, C-CDAMs, G-CDAMs, and O-CDAMs. h) Afterglow decay curves of B-CDAMs, C-CDAMs, G-CDAMs, and O-CDAMs under the optimal excitation at 260 nm, 440 nm, 340 nm, 440 nm, respectively.

The hexagonal $NaYF_4$:Yb,Tm UMs with intense UCL were prepared by a simple hydrothermal method (see the experimental section in the Supporting Information). The as-prepared UMs present an average size of about 570 × 310 nm, and the HRTEM image shows clear lattice fringes with the spacing of 0.30 nm, corresponding to the interplanar d-spacing of (110) planes of hexagonal $NaYF_4$ (Figure S8a). X-ray diffraction (XRD) peaks of the UMs in Figure S8b match well with the standard hexagonal $NaYF_4$ (JCPDS No. 16-0334), which is consistent with the HRTEM result. At the same time, the optical properties of $NaYF_4$:Yb,Tm were measured. As shown in Figure S9a, the UCL emission peaks of the prepared UMs are located at 345 nm, 362 nm, 451 nm, 478 nm, and 647 nm, respectively. The electronic transitions between different energy levels of Tm^{3+} corresponding to the five UCL emission peaks are: $^1I_6 \rightarrow {}^3F_4$, $^1D_2 \rightarrow {}^3H_6$, $^1D_2 \rightarrow {}^3F_4$, $^1G_4 \rightarrow {}^3H_6$, and $^1G_4 \rightarrow {}^3F_4$, respectively (Figure 2a).[22] The UCL lifetimes of Tm^{3+} monitored at the five UCL emission peaks were: 254 μs, 302 μs, 298 μs, 581 μs, and 582 μs, respectively (Figure S9b). Note that $NaYF_4$:Yb,Tm UMs can be selected as the energy donors to excite the CDAMs because there were notable spectral overlaps between UCL of the UMs and absorption of the CDAMs (Figure S10), which satisfied the necessary conditions of an efficient energy transfer.

To activate the multicolor afterglow of the CDAMs under NIR excitation through efficient energy transfer (Figure 2a), we dispersed $NaYF_4$:Yb,Tm UMs and CDAMs together in acetic acid, and UM/CDAMs were obtained after sufficient stirring, precipitation, and drying. The TEM images of UM/CDAMs can be seen in Figure S11. As expected, the bright and persistent multicolor afterglow were activated in UM/CDAMs after turning off the NIR CW laser at 980 nm, and they could be observed by naked eyes for 7 s, 6 s, 5 s, and 0.5 s, respectively (Figure 2b and Video 1-4). Intriguingly, we were surprised to find that the UM/C-CDAMs showed time-dependent afterglow colors after 4 s. The time-resolved afterglow spectra of UM/C-CDAMs and the corresponding color coordinates also confirmed the existence of the time-dependent afterglow colors (Figure S12). The phenomenon of color change could be caused by the different decay rates of the two luminescence centers corresponding to dual emission peaks (Figure S13).[23] Moreover, the UV-excited afterglow images (Figure 2b) of UM/CDAMs and the corresponding afterglow emission spectra (Figure S14) proved that the original optical properties of CDAMs had not been changed after the addition of UMs. The normalized afterglow emission spectra of

UM/CDAMs showed four main emission band centered at 455 nm, 485 nm, 519 nm, and 605 nm, respectively (Figure 2c), corresponding to the color coordinates changed from blue to orange regions in the CIE (Commission Internationale de l'Eclairage) 1931 chromaticity diagram (Figure 2d). In addition, the afterglow decay curves of UM/CDAMs can been seen in Figure S15.

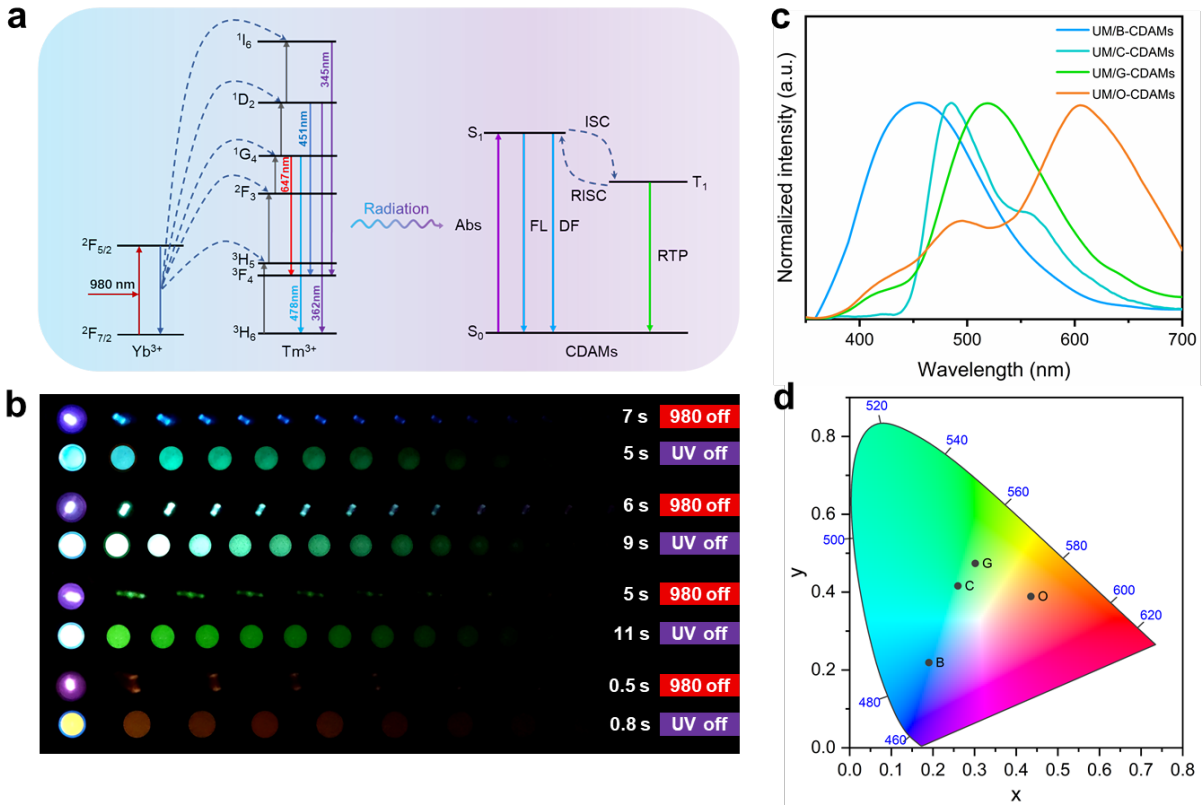

Figure 2. a) Energy level diagram of $NaYF_4$:Yb,Tm UMs and CDAMs, and schematic illustration of activating the multicolor afterglow of the CDAMs under NIR excitation through efficient energy transfer. b) Photographs of UM/B-CDAMs, UM/C-CDAMs, UM/G-CDAMs, and UM/O-CDAMs with the NIR CW laser on and off at 980 nm. c) Normalized afterglow emission spectra of UM/B-CDAMs, UM/C-CDAMs, UM/G-CDAMs, and UM/O-CDAMs under the NIR CW laser excitation at 980 nm. d) CIE coordinates of the afterglow emission of UM/B-CDAMs, UM/C-CDAMs, UM/G-CDAMs, and UM/O-CDAMs under the NIR CW laser excitation at 980 nm.

In a set of detailed experiments, we explored the optimal conditions that affect the afterglow intensity of UM/CDAMs. First of all, we found that the UCL intensity of UMs showed a trend from rising to declining when we increased the doping ratio of Yb^{3+} from 20 mol% to 80 mol% in the UMs (Figure S16a). The corresponding afterglow emission spectrum displayed the same trend, with the intensity

reaching the maximum at 60 mol% Yb^{3+} (Figure 3a and Figure S16b), which also illustrated the occurrence of energy transfer from UMs to CDAMs. Hereafter, the afterglow emission of UM/CDAMs was optimized by controlling the ratio of UMs to CDAMs. With the ratio of the CDAMs increasing, the afterglow emission intensity showed a tendency from increasing to decreasing (Figure 3b and Figure S17). The reason for the decreasing trend was that the limited UMs were not enough to fully excite all the CDAMs, resulting in the decreasing average apparent intensity for UM/CDAMs.

In order to get more profound insights into the mechanism of energy transfer, we characterized the steady-state and transient properties of UM/CDAMs. As shown in Figure S18, as the ratio of the CDAMs increased by a certain extent, the integrated intensity of UV and blue emissions of Tm^{3+} maintained the overall downward trend, which is the result of energy transfer from UMs to CDAMs. As observed from Figure S19, the calculated energy transfer efficiency in all UM/CDAMs increases gradually because of more absorption with increasing CDAMs. In addition, the energy transfer efficiency of UM/C-CDAMs is the highest one, which can be attributed to the fact that UMs and C-CDAMs have the largest degree of spectral overlaps (Figure S10). To further determine the type of energy transfer, we investigated the UCL lifetimes of UM/CDAMs via UCL decay curves. It is worth noting that the reduction in the UCL lifetime of the energy donor is an essential sign for non-radiative energy transfer due to the imposed extra relaxation approach on the donor.[24] As observed from Figure 3c and Figure S20, the UCL decay curves monitored at each emission wavelength (345 nm, 362 nm, 451 nm, 478 nm, and 647 nm) of Tm^{3+} have nearly perfect overlaps with the varying ratio of UMs to C-CDAMs, indicating the unaltered UCL lifetimes of UM/C-CDAMs in contrast with the pure UMs (Figure 3d). Consistent situations also occurred for other UM/CDAMs, as seen from Figure S21-S23. Furthermore, the UCL lifetimes of UM/CDAMs containing various CDAMs with a certain ratio (1:2) were also almost unchanged (Figure 3e-f and Figure S24), as a convinced result of radiative energy transfer instead of non-radiative energy transfer. In short, the energy transfer mechanism can be explained as follows. Yb^{3+} as the sensitizer absorbed the 980 nm NIR light and transferred energy to the $^1I_6$, $^1D_2$, and $^1G_4$ levels of the Tm^{3+}. With the radiative transitions of $^1I_6$, $^1D_2$, and $^1G_4$ levels, the released radiative energy photons were absorbed by the CDAMs to generate singlet excitons (S_1). Afterward, the singlet excitons were converted to triplet excitons (T_1) through intersystem crossing (ISC), and the phosphorescent emission can be observed when the triplet excitons transfer back to the ground state S_0. If the reverse intersystem crossing (RISC) occurs, the delayed fluorescence will be seen as shown in Figure 2a.

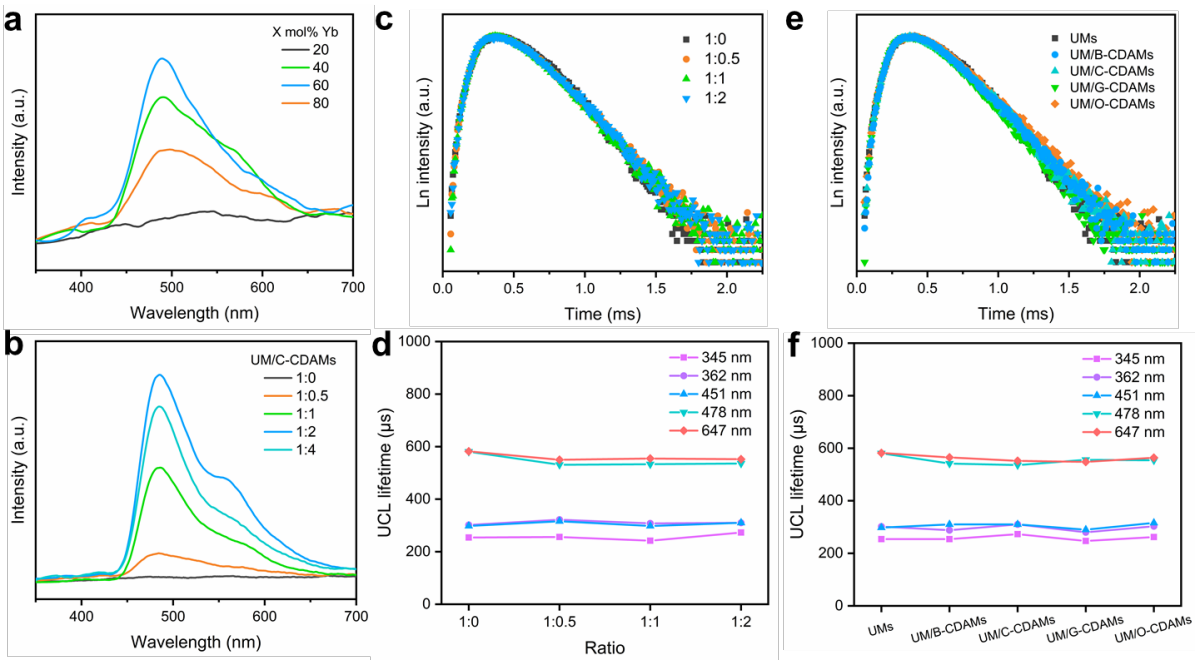

Figure 3. a) The afterglow emission spectra of UM/C-CDAMs with the varying doping ratio of Yb^{3+} under the NIR CW laser excitation at 980 nm. b) The afterglow emission spectra of UM/C-CDAMs with the varying ratio of UMs to CDAMs under the NIR CW laser excitation at 980 nm. c) The UCL decay curves of UM/C-CDAMs with the varying ratio of UMs to C-CDAMs monitored at 362 nm under the NIR CW laser excitation at 980 nm. d) The UCL lifetime of UM/C-CDAMs at the corresponding emission wavelength (345 nm, 362 nm, 451 nm, 478 nm, 647nm). e) The UCL decay curves of UM/CDAMs with the various CDAMs at a certain ratio (1:2) monitored at 362 nm under the NIR CW laser excitation at 980 nm. f) The UCL lifetimes of UM/CDAMs at the corresponding emission wavelength (345 nm, 362 nm, 451 nm, 478 nm, and 647 nm).

The unique NIR-excited multicolor afterglow properties of these UM/CDAMs offer opportunities for multifunctional applications such as fingerprint recognition, 4D code, and optical anti-counterfeiting signatures. As we all know, fingerprints are unique and immutable, and are regarded as another ID card for human beings. Fingerprint recognition, as a convenient, effective and safe feature identification technology, plays an important role in the field of the criminal investigation. Traditional fluorescent materials are sometimes insensitive because of the interference from the background fluorescence in fingerprint recognition, whereas afterglow materials can avoid the influence of environmental factors. Herein, the fully ground UM/CDAMs powders were evenly covered on the surface of latent fingerprints and kept for a while, and then the dyed fingerprints were obtained after carefully removing the excess powders (Figure 4a I-III). After turning off the 365 nm UV light, we can clearly see the visual fingerprints

with plain whorl through blue, cyan, and green afterglow images captured by a mobile phone (Figure 4a IV-VI). Furthermore, Figure 4 VIII-XI displayed some fine details such as core, termination, pore, island, and bifurcation after turning off the 980 nm NIR laser, which was consistent with the UV-excited afterglow image of the corresponding area in Figure 4a VII (h-k). These fine details provided convinced characteristic information for fingerprint identification, and so clear and detailed results were rarely seen in other reports. In short, the fast fingerprint recognition based on UM/CDAMs has high contrast and sensitivity, which is extremely advantageous to visual fingerprint analysis and detection. Meantime, the multicolor afterglow has tremendous application prospects in information code. As shown in Figure 4b, the time-resolved dynamic colorful matrix modules are made up of some patterns with different afterglow colors, thereby they were called 4D code.[25] The matrix modules with afterglow at different time points are independent 3D codes under the NIR CW laser irradiation at 980 nm, and they can carry different information. As shown in Figure 4c, code 1, code 3, and code 5 export error, while code 2 and code 4 can read out info A and info B, respectively. And the integration of all 3D codes can encode info C as a more advanced and safer 4D code. Note that permutation and combination of different 3D codes can encode more information. Therefore, the 4D code system can store a large amount of encrypted information. In addition, the colorful afterglow can be applied to advanced optical anti-counterfeiting signatures by laser writing without any traces (Figure 4d). Using the 980 nm CW laser as the 'pen', the multicolor afterglow as the 'ink', and UM/CDAMs as the 'canvas', a masterpiece '*Invitation to Wine*' by Li Bai (a great poet in the Tang Dynasty, China) came into our sight (Figure 4e and Video 5).

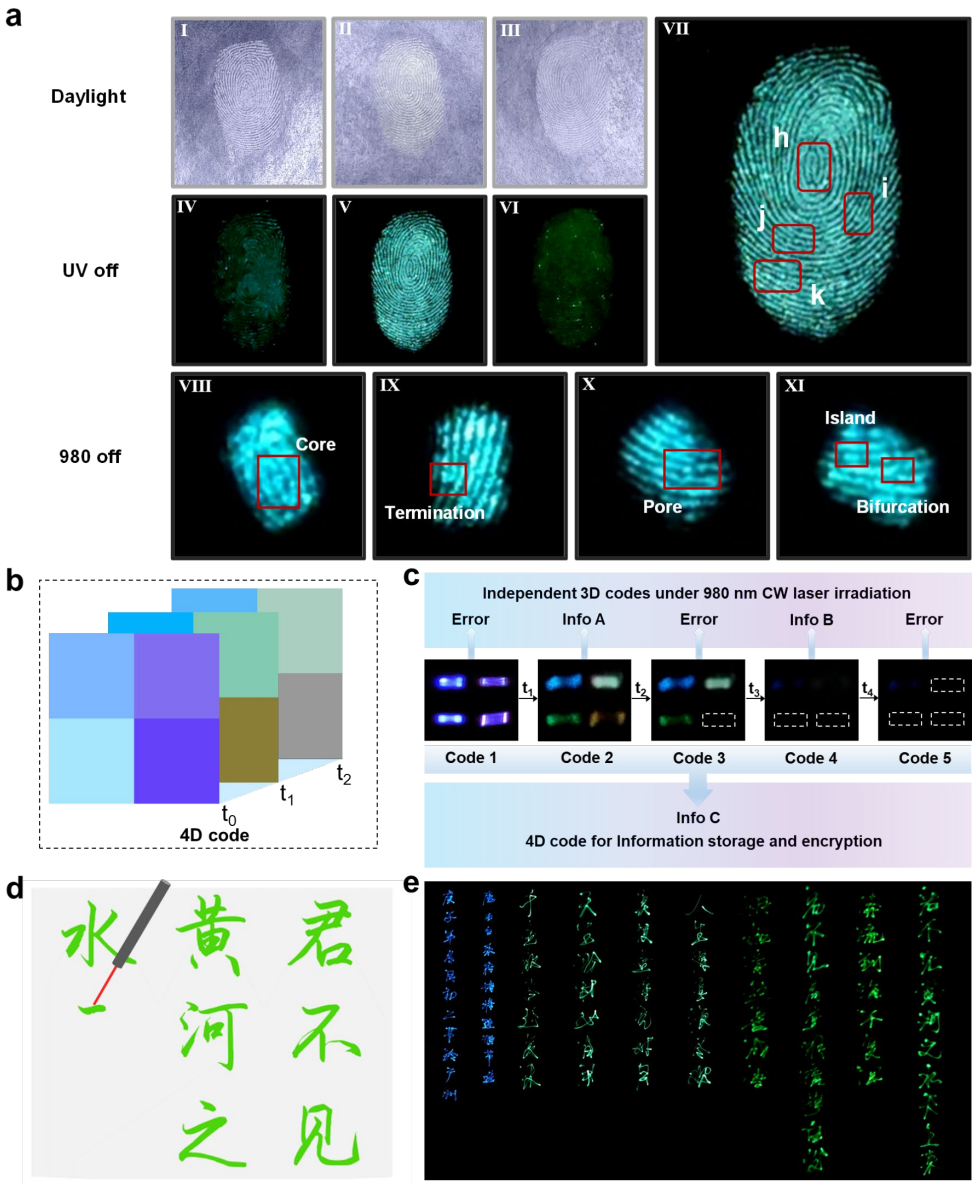

Figure 4. a) Visualized afterglow images of latent fingerprints under daylight (I-III), and UV light off (IV-VI); (VII) the enlarged image of V, and (VIII-XI) the afterglow images of the corresponding area in VII (h-k) under 980 nm laser off. b) Schematic illustration of 4D code. c) The simplified formation process of the 4D code, in which afterglow images of the matrix modules were captured at different times under 980 nm CW laser irradiation on (code 1) and off (code 2-5), respectively. d) Schematic illustration of laser writing. e) Photographs of laser writing, in which each word was displayed through a 980 nm laser-excited afterglow image. Note that all the above photographs were taken with a mobile phone.

In summary, we have reported a novel and universal method to achieve NIR-excited multicolor afterglow in CDAMs. The mechanism of radiative energy transfer keeps efficient energy transfer free from distance restriction compared with non-radiative FRET. Therefore, it is quite easy and convenient

to activate the multicolor afterglow of CDAMs under NIR excitation just through the full mixing of UMs and CDAMs. The investigation results suggest that the strategy we proposed is universal in the field of CDAMs. Due to the unique NIR-excited multicolor afterglow, multiple applications are demonstrated for fingerprint recognition, 4D code and optical anti-counterfeiting signatures. More importantly, this work finds a way out of the dilemma that CDAMs cannot be excited by NIR light, and creates a promising alternative to the currently reported UV-excited CDAMs. Finally, it is expected to advance more works such as time-dependent afterglow colors and water-soluble property, for ease of application in advanced anti-counterfeiting and afterglow bioimaging.

Acknowledgements

This work was supported by the National Natural Science Foundation of China (51602108 and 52073242), the Guangdong Basic and Applied Basic Research Foundation (2020A1515011210), Science and Technology Planning Project of Guangzhou City (202007020005, 202102080288). W.-Y. W. would also like to thank the Hong Kong Research Grants Council (PolyU 153058/19P), Hong Kong Polytechnic University (1-ZE1C), and the Endowed Professorship in Energy from Ms. Clarea Au (847S) for the financial support. We thank Prof. Zhenguo Chi (Sun Yat-Sen University), Dr. Zhan Yang (Sun Yat-Sen University), Prof. Yixi Zhuang (Xiamen University) and Prof. Yang Li (Guangzhou Medical University) for their assistance in the measurements of the NIR-excited afterglow emission spectra, time-resolved afterglow spectra, and afterglow decay curves.

Conflict of interest

The authors declare no conflict of interest.

Keywords: carbon dots • energy transfer • near-infrared-excited material • room-temperature afterglow • upconversion

[1] a) R. Kabe, C. Adachi, *Nature* **2017**, *550*, 384-387; b) W. Zhao, Z. He, B. Z. Tang, *Nat. Rev. Mater.* **2020**, *5*, 869-885; c) G. Baryshnikov, B. Minaev, H. Agren, *Chem. Rev.* **2017**, *117*, 6500-6537; d) T. Zhang, X. Ma, H. Wu, L. Zhu, Y. Zhao, H. Tian, *Angew. Chem. Int. Ed.* **2020**, *59*, 11206-11216; *Angew. Chem.* **2020**, *132*, 11302-11312; e) N. Gan, H. Shi, Z. An, W. Huang, *Adv. Funct. Mater.* **2018**, *28*, 1802657.

[2] Z. An, C. Zheng, Y. Tao, R. Chen, H. Shi, T. Chen, Z. Wang, H. Li, R. Deng, X. Liu, W. Huang, *Nat. Mater.* **2015**, *14*, 685-690.

[3] a) L. Gu, H. Shi, L. Bian, M. Gu, K. Ling, X. Wang, H. Ma, S. Cai, W. Ning, L. Fu, H. Wang, S. Wang, Y. Gao, W. Yao, F. Huo, Y. Tao, Z. An, X. Liu, W. Huang, *Nat. Photonics.* **2019**, *13*, 406-411; b) P. Lehner, C. Staudinger, S. M. Borisov, I. Klimant, *Nat. Commun.* **2014**, *5*, 4460; c) H. Li, S. Ye, J. Guo, J. Kong, J. Song, Z. Kang, J. Qu, *J. Mater. Chem. C* **2019**, *7*, 10605-10612; d) J. Wang, X. Gu, H. Ma, Q. Peng, X. Huang, X. Zheng, S. H. P. Sung, G. Shan, J. W. Y. Lam, Z. Shuai, B. Z. Tang, *Nat. Commun.* **2018**, *9*, 2963; e) Q. Miao, C. Xie, X. Zhen, Y. Lyu, H. Duan, X. Liu, J. V. Jokerst, K. Pu, *Nat. Biotechnol.* **2017**, *35*, 1102-1110.

[4] a) J. Liu, R. Li, B. Yang, *ACS Cent. Sci.* **2020**, *6*, 2179-2195; b) A. Xu, G. Wang, Y. Li, H. Dong, S. Yang, P. He, G. Ding, *Small* **2020**, *16*, 2004621; c) K. Jiang, Y. Wang, Z. Li, H. Lin, *Mater. Chem. Front.* **2020**, *4*, 386-399. d) Y. Sun, X. Zhang, J. Zhuang, H. Zhang, C. Hu, M. Zheng, B. Lei, Y. Liu, *Carbon* **2020**, *165*, 306-316.

[5] a) K. Jiang, S. Hu, Y. Wang, Z. Li, H. Lin, *Small* **2020**, *16*, 2001909; b) S. Song, L. Sui, K. Liu, Q. Cao, W. Zhao, Y. Liang, C. Lv, J. Zang, Y. Shang, Q. Lou, X. Yang, L. Dong, K. Yuan, C. Shan, *Nano Res.* DOI: 10.1007/s12274-020-3204-z; c) K. Jiang, Y. Wang, X. Gao, C. Cai, H. Lin, *Angew. Chem. Int. Ed.* **2018**, *57*, 6216-6220; *Angew. Chem.* **2018**, *130*, 6324-6328; d) Y. Sun, S. Liu, L. Sun, S. Wu, G. Hu, X. Pang, A. T. Smith, C. Hu, S. Zeng, W. Wang, Y. Liu, M. Zheng, *Nat. Commun.* **2020**, *11*, 5591; e) K. Jiang, X. Gao, X. Feng, Y. Wang, Z. Li, H. Lin, *Angew. Chem. Int. Ed.* **2020**, *59*, 1263-1269; Angew. Chem. **2020**, *132*, 1279-1285; f) Y. Liang, S. Gou, K. Liu, W. Wu, C. Guo, S. Lu, J. Zang, X. Wu, Q. Lou, L. Dong, Y. Gao, C. Shan, *Nano Today* **2020**, *34*, 100900; g) S. Tao, S. Lu, Y. Geng, S. Zhu, S. A. T. Redfern, Y. Song, T. Feng, W. Xu, B. Yang, *Angew. Chem. Int. Ed.* **2018**, *57*, 2393-2398; *Angew. Chem.* **2018**, *130*, 2417-2422; h) P. Long, Y. Feng, C. Cao, Y. Li, J. Han, S. Li, C. Peng, Z. Li, W. Feng, *Adv. Funct. Mater.* **2018**, *28*, 1800791; i) Q. Feng, Z. Xie, M. Zheng, *Chem. Eng. J.* **2021**, *420*, 127647; j) C. Xia, S. Zhu, S. Zhang, Q. Zeng, S. Tao, X. Tian, Y. Li, B. Yang, *ACS Appl. Mater. Interfaces* **2020**, *12*, 38593-38601.

[6] a) Z. Tian, D. Li, E. V. Ushakova, V. G. Maslov, D. Zhou, P. Jing, D. Shen, S. Qu, A. L. Rogach, *Adv. Sci.* **2018**, *5*, 1800795; b) J. Zhu, X. Bai, X. Chen, H. Shao, Y. Zhai, G. Pan, H. Zhang, E. V. Ushakova, Y. Zhang, H. Song, A. L. Rogach, *Adv. Opt. Mater.* **2019**, *7*, 1801599; c) Y. Liu, X. Huang, Z. Niu, D. Wang, H. Gou, Q. Liao, K. Xi, Z. An, X. Jia, *Chem. Sci.* **2021**, *12*, 8199-8206. d) J. Tan, R. Zou, J. Zhang, W. Li, L. Zhang, D. Yue, *Nanoscale* **2016**, *8*, 4742-4747. e) Y. Deng, D. Zhao, X. Chen, F. Wang, H. Song, D. Shen, *Chem. Commun.* **2013**, *49*, 5751-5753.

[7] Y. Gao, H. Zhang, Y. Jiao, W. Lu, Y. Liu, H. Han, X. Gong, S. Shuang, C. Dong, *Chem. Mater.* **2019**, *31*, 7979-7986.

[8] Q. Li, M. Zhou, M. Yang, Q. Yang, Z. Zhang, J. Shi, *Nat. Commun.* **2018**, *9*, 734.

[9] H. Liu, F. Wang, Y. Wang, J. Mei, D. Zhao, *ACS Appl. Mater. Interfaces* **2017**, *9*, 18248-18253.

[10] J. Joseph, A. A. Anappara, *ChemistrySelect* **2017**, *2*, 4058-4062.

[11] a) B. Wang, Y. Mu, H. Zhang, H. Shi, G. Chen, Y. Yu, Z. Yang, J. Li, J. Yu, *ACS Cent. Sci.* **2019**, *5*, 349-356; b) J. Liu, H. Zhang, N. Wang, Y. Yu, Y. Cui, J. Li, J. Yu, *ACS Mater. Lett.* **2019**, *1*, 58-63. c) B. Wang, Y. Yu, H. Zhang, Y. Xuan, G. Chen, W. Ma, J. Li, J. Yu, *Angew. Chem. Int. Ed.* **2019**, *58*, 18443-18448; *Angew. Chem.* **2019**, *131*,18614-18619;

[12] a) W. Shi, J. Yao, L. Bai, C. Lu, *Adv. Funct. Mater.* **2018**, *28*, 1804961; b) L. Bai, N. Xue, Y. Zhao, X. Wang, C. Lu, W. Shi, *Nano Res.* **2018**, *11*, 2034-2045.
[13] a) Y. C. Liang, K. K. Liu, X. Y. Wu, Q. Lou, L. Z. Sui, L. Dong, K. J. Yuan, C. X. Shan, *Adv. Sci.* **2021**, *8*, 2003433; b) J. He, Y. Chen, Y. He, X. Xu, B. Lei, H. Zhang, J. Zhuang, C. Hu, Y. Liu, *Small* **2020**, *16*, 2005228; c) W. Li, S. Wu, X. Xu, J. Zhuang, H. Zhang, X. Zhang, C. Hu, B. Lei, C. F. Kaminski, Y. Liu, *Chem. Mater.* **2019**, *31*, 9887-9894; d) K. Jiang, Y. Wang, C. Cai, H. Lin, *Chem. Mater.* **2017**, *29*, 4866-4873.
[14] a) Q. Li, M. Zhou, Q. Yang, Q. Wu, J. Shi, A. Gong, M. Yang, *Chem. Mater.* **2016**, *28*, 8221-8227; b) C. Lin, Y. Zhuang, W. Li, T. L. Zhou, R. J. Xie, *Nanoscale* **2019**, *11*, 6584-6590.
[15] W. Li, W. Zhou, Z. Zhou, H. Zhang, X. Zhang, J. Zhuang, Y. Liu, B. Lei, C. Hu, *Angew. Chem. Int. Ed.* **2019**, *58*, 7278-7283; *Angew. Chem.* **2019**, *131*, 7356-7361.
[16] C. Wang, Y. Chen, T. Hu, Y. Chang, G. Ran, M. Wang, Q. Song, *Nanoscale* **2019**, *11*, 11967-11974.
[17] a) Z. Xu, X. Sun, P. Ma, Y. Chen, W. Pan, J. Wang, *J. Mater. Chem. C* **2020**, *8*, 4557-4563; b) Y. Gao, H. Zhang, S. Shuang, C. Dong, *Adv. Opt. Mater.* **2020**, *8*, 1901557; c) W. He, X. Sun, X. Cao, *ACS Sustain. Chem. Eng.* **2021**, *9*, 4477-4486.
[18] a) G. Hong, A. L. Antaris, H. Dai, *Nat. Biomed. Eng.* **2017**, *1*; b) H. M. Kim, B. R. Cho, *Chem. Rev.* **2015**, *115*, 5014-5055; c) Kenry, Y. Duan, B. Liu, *Adv .Mater.* **2018**, *30*, 1802394; d) Z. Wang, C. Y. Zhu, S. Y. Yin, Z. W. Wei, J. H. Zhang, Y. N. Fan, J. J. Jiang, M. Pan, C. Y. Su, *Angew. Chem. Int. Ed.* **2019**, *58*, 3481-3485; *Angew. Chem.* **2019**, *131*, 3519-3523; e) X. Ji, L. Ge, C. Liu, Z. Tang, Y. Xiao, Z. Lei, W. Gao, S. Blake, D. De, X. Zeng, N. Kong, X. Zhang, W. Tao. *Nat. Commun*. **2021**, *12*, 1124; f) D. Gao, T. Chen, Y. Han, S. Chen, Y. Wang, X. Guo, H. Wang, X. Chen, M. Guo, Y. S. Zhang, G. Hong, X. Zhang, Z. Tian, Z. Yang. *Nano-Micro Lett*. **2021**,*13*, 99; Z. Yang, D. Gao, X. Guo, L. Jin, J. Zhang, Y. Wang, S. Chen, X. Zheng, L. Zeng, M. Guo, X. Zhang, Z. Tian. *ACS Nano*, **2020**, *14*, 17442-17457.
[19] a) L. Ruan, Y. Zhang, *Nat. Commun.* **2021**, *12*, 219; b) S. Liu, J. Huang, L. Yan, N. Song, P. Zhang, J. He, B. Zhou, *J. Mater. Chem. A* **2021**, *9*, 4007-4017; c) B. Zhou, L. Yan, L. Tao, N. Song, M. Wu, T. Wang, Q. Zhang, *Adv. Sci.* **2018**, *5*, 1700667.
[20] T. F. Yeh, C. Y. Teng, S. J. Chen, H. Teng, *Adv. Mater.* **2014**, *26*, 3297-3303.
[21] a) L. Jiang, H. Ding, S. Lu, T.Geng, G. Xiao, B. Zou, H. Bi, *Angew. Chem. Int. Ed.* **2020**, *59*, 9986-9991; *Angew. Chem.* **2020**, *132*, 10072-10077; b) L. Jiang, H. Ding, M. Xu, X. Hu, S. Li, M. Zhang, Q. Zhang, Q. Wang, S. Lu, Y. Tian, H. Bi, *Small* **2020**, *16*, 2000680; c) H. Ding, J. Xu, L. Jiang, C. Dong, Q. Meng, S. u. Rehmanb, J. Wang, Z Ge, V. Y. Osipova, H. Bi, *Chinese Chem. Lett.* DOI: 10.1016/j.cclet.2021.04.033.
[22] a) J. Zhou, Z. Liu, F. Li, *Chem. Soc. Rev.* **2012**, *41*, 1323-1349; b) F. Wang, X. Liu, *J. Am. Chem. Soc.* **2008**, *130*, 5642-5643.
[23] J. Tan, Q. Li, S. Meng, Y. Li, J. Yang, Y. Ye, Z. Tang, S. Qu, X. Ren, *Adv. Mater.* **2021**, *33*, 2006781.
[24] a) D. Tu, L. Liu, Q. Ju, Y. Liu, H. Zhu, R. Li, X. Chen, *Angew. Chem. Int. Ed.* **2011**, *50*, 6306-6310; *Angew. Chem.* **2011**, *123*, 6430-6434; b) J. Gu, J. Shen, L. Sun, C. Yan, *J. Phys. Chem. C* **2008**, *112*, 6589-6593.
[25] X. Wang, H. Ma, M. Gu, C. Lin, N. Gan, Z. Xie, H. Wang, L. Bian, L. Fu, S. Cai, Z. Chi, W. Yao, Z. An, H. Shi, W. Huang, *Chem. Mater.* **2019**, *31*, 5584-5591.

Entry for the Table of Contents

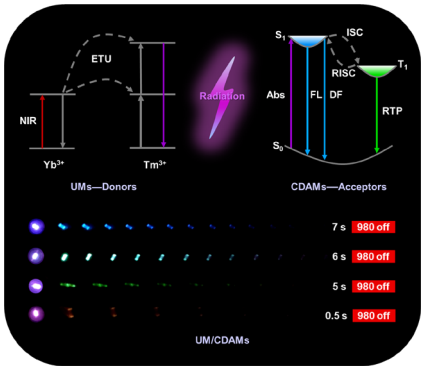

A universal method is firstly developed to activate near-infrared-excited multicolor afterglow of carbon dots-based RTA materials (CDAMs) through radiative energy from $NaYF_4$:Yb,Tm upconversion materials (UMs). Excitingly, the resulting UM/CDAMs demonstrates bright and persistent afterglow from blue to orange under the NIR CW laser excitation at 980 nm.